Purely antiferromagnetic frustrated Heisenberg model in the spin-ladder compound BaFe₂Se₃

A. Roll [1,2] S. Petit,[2] A. Forget [3] D. Colson,[3] A. Banerjee,[4,5] P. Foury-Leleykian,[1] and V. Balédent [1,*]

[1]*Laboratoire de Physique des Solides, Université Paris-Saclay, CNRS, 91405 Orsay, France*

[2]*Laboratoire Léon Brillouin, CEA, CNRS, Université Paris-Saclay, 91191 Gif sur Yvette, France*

[3]*Université Paris-Saclay, CEA, CNRS, SPEC, 91191 Gif-sur-Yvette, France*

[4]*Department of Physics and Astronomy, Purdue University, West Lafayette, Indiana 47906, USA*

[5]*Neutron Scattering Division, Oak Ridge National Laboratory, Oak Ridge, Tennessee 37831, USA*

The spin dynamics in the block magnetic phase of the iron-based ladder compound BaFe₂Se₃ has been studied by means of single-crystal inelastic neutron scattering. Using linear spin-wave theory and Monte Carlo simulations, our analysis points to a magnetic Heisenberg model with effective frustrated antiferromagnetic couplings only, able to describe both the exotic block order and its dynamics. This new and purely antiferromagnetic picture offers a fruitful perspective to describe multiferroic properties, but also understand the origin of the stripelike magnetic instability observed under pressure as well as in other parent compounds with similar crystalline structure.

I. INTRODUCTION

Magnetism plays a prominent role in many exotic properties of condensed matter from unconventional superconductivity to multiferroicity and spin liquid phases. Copper has long been the focus of attention for studying these exotic phases, thanks to its half-integer spin, which promotes the emergence of these quantum states. On the other hand, research on multiferroicity has focused on manganese-based compounds, whose large magnetic moment has made it possible to obtain sufficiently strong magnetoelectric couplings to allow applications. More recently, iron-based compounds have found a place at the interface between these two paradigms. Indeed, unconventional superconductivity has been discovered in pnictides, and the large iron magnetic moment combined with magnetic interactions allows to obtain multiferroic materials at quite high temperatures. BaFe₂Se₃ embodies this new path, by showing multiferroic properties below 250 K, and superconductivity above 10 GPa (see phase diagram Fig. 1).

At ambient pressure, BaFe₂Se₃ crystallizes in the polar Pm space group [1,2] with a weak distortion from the average Pnma space group. For sake of clarity, we will use the orthorhombic average space group in which there are two ladders per unit cell, each formed by two adjacent legs running along the b axis. Below $T_N = 250$ K, an exotic magnetic order develops, called "block order", consisting in an antiferromagnetic arrangement of square blocks of four parallel iron spins, pointing mainly along the a direction, i.e., perpendicular to the ladders. Along the legs, the structure, thus, shows an up-up-down-down pattern [3]. This model has been refined using single-crystal neutron diffraction, revealing a tilt

of the moments with respect to the a axis, and resulting in an umbrellalike magnetic order [4]. Under pressure, this exotic magnetic state gives way to a more conventional order consisting in stripes of an up-down-up-down pattern along the legs [5], and analogous to the one observed in parent compounds with similar crystalline structure. It is worth noting that this classical up-down-up-down pattern is also stable close to the superconducting dome (see dark-green region in Fig. 1).

Understanding the magnetic couplings, at the heart of the different properties of this compound, requires the study of its excitations. On the basis of a first inelastic neutron-scattering measurement performed on powder samples, the authors of Ref. [7] have suggested an alternation of ferromagnetic and antiferromagnetic couplings along the legs. Although this model clearly stabilizes the correct magnetic structure due to the absence of magnetic frustration, it raises several questions. Although the exchange paths are admittedly different between up-up and up-down iron bonds along a given leg [2], they hardly justify the change in both sign and amplitude, hence, the nature of the exchange interactions, as also underlined in theoretical literature on spin dynamics [8]. Furthermore, the ferromagnetic nature of some interactions seems incompatible with the Goodenough-Kanamori orbital rules: As the Fe-Se-Fe angle (denoted by ψ) strongly departs from 90° (see Table I), the antiferromagnetic superexchange is expected to prevail over the ferromagnetic direct coupling. Another physical argument in favor of purely antiferromagnetic bonds along the ladder is the vicinity of the classical antiferromagnetic up-down-up-down order observed under moderate pressure (4 GPa) and in all other members of the family presenting a similar crystalline structure, such as KFe₂Se₃, CsFe₂Se₃, and BaFe₂S₃ [3,9,10].

In this paper, we present new inelastic neutron-scattering (INS) measurements performed on a single crystal of BaFe₂Se₃ providing unique details on the spin-wave

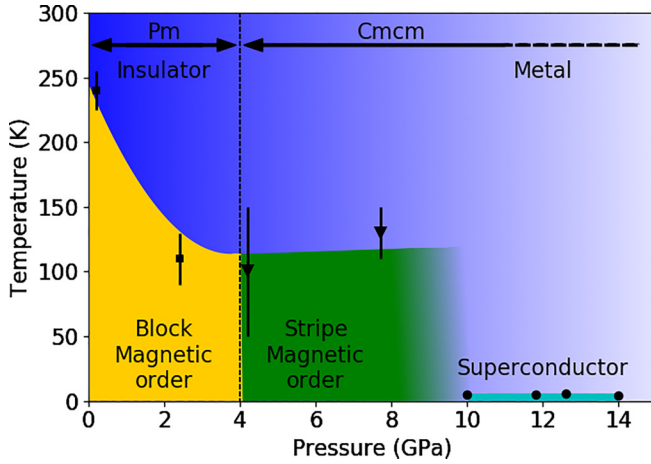*Corresponding author: victor.baledent@universite-paris-saclay.fr

FIG. 1. Schematic pressure temperature phase diagram of BaFe$_2$Se$_3$. The block order (up-up-down-down) occupies the yellow region (black squares), whereas, the stripe order (up-down-up-down) is observed in the green region (black triangles). Superconductivity appears above 10 GPa (black circles from Refs. [5,6]). The structural transition from the *Pm* to the *Cmcm* space group is observed at 4 GPa, and progressive metallization occurs between 4 and 10 GPa.

dispersion. The modeling of the data leads to a purely antiferromagnetic Heisenberg-Hamiltonian, allowing one to describe both the magnetic order and the dynamics. This picture also provides a natural understanding of the evolution of the magnetism under pressure as well as the magnetic ground state of parent compounds.

II. EXPERIMENT AND ANALYSIS

Single crystals were grown following the method described in Ref. [1] and fully characterized [11]. The INS experiments were carried out on the wide angular-range time-of-flight chopper spectrometer (ARCS) at the Spallation Neutron Source, Oak Ridge National Laboratory (ORNL). The measurements were conducted at 20 K with incident beam energies $E_i = 25$ and 125 meV yielding an energy resolution of about 1 and 6 meV, respectively. Slices were taken from the full (Q, ω) dataset to produce maps as a function of energy transfer ω and wave-vector Q along the three main crystallographic directions a–c. Only dispersion along the b direction, corresponding to the ladder, was visible, as expected for a quasiunidimensional system [11]. This allowed to integrate along the other directions to improve statistics. The measured dispersion obtained with $E_i = 125$ meV at 20 K along (1/2, K, and 1/2) is shown in Fig. 2(a). An acoustic mode is clearly visible, dispersing up to 60 meV. The data

TABLE I. Angles (in degrees) between the Fe-Se-Fe bonds for the different possible paths within the ladder, according to the structure published in Ref. [1]. The couplings correspond to the exchange interactions affected by these angles, as represented in Fig. 2(g).

$\psi_{\text{Fe-Se-Fe}}$	66(7)	71(6)	65.8(19)	101(3)	105(3)
Involved coupling	J_1	J_1'	J_R	J_2	J_2'

obtained with $E_i = 25$ meV allows a closer look at the low-energy part. By subtracting the elastic part [11], a gap is evidenced in the energy cut at $Q = (1/2, 1/2, \text{and } 1/2)$ as shown in Fig. 2(b). The gap value around 6 meV is in good agreement with the one inferred from powder sample data [7]. At higher energy, three dispersionless optical modes are observed. In order to make them more visible, an integration along H ($\Delta H = 0.5$), K ($\Delta K = 0.5$), and L ($\Delta L = 10$) was performed, yielding the energy dependence displayed in Fig. 2(c). They appear at 92(2), 101(2), and 110(2) meV. Only two of these modes were resolved in the powder experiment [7], providing a strong additional constraint on the subsequent modeling.

To model the spin dynamics, an exhaustive survey of the structures stabilized by different sets of couplings is necessary. To this end, classical Monte Carlo was used to determine the phase diagram of a single ladder (see the details in Ref. [11]). To describe the system, we used the following Heisenberg model:

$$H_{\text{mag}} = \sum_{i<j} J_{ij}\mathbf{S}_i \cdot \mathbf{S}_j + \frac{3}{2}D\sum_i (\mathbf{S}_i \cdot \mathbf{n}_i)^2, \qquad (1)$$

the first sum runs over iron magnetic ions, $\mathbf{S}_i$'s denote the spin at site i, and J_{ij}'s are exchange integrals between spins at different sites. As sketched in Fig. 2(g), J_1 and J_1' correspond to nearest-neighbor interactions, and J_3 corresponds to next-nearest-neighbor interactions within a given leg of the ladder. These couplings may lead to frustration in a purely antiferromagnetic model. J_R, J_2, and J_2' couple nearest- and next-nearest-neighbor spins, respectively, in adjacent legs. The second sum describes the magnetic anisotropy: $3D/2$ is the single-ion anisotropy, and $\mathbf{n}_i$ defines the local anisotropy axis. The results of our calculations are presented in Fig. 3 with maps of the propagation vector value as a function of the various couplings in units of J_3. The unit of the propagation vector is defined by a lattice consisting of a single magnetic site per unit cell. This means that the purely antiferromagnetic order corresponds to $k_y = 0.5$ (doubling of the unit cell), and the block order with four spins per unit cell corresponds to $k_y = 0.25$. As can be intuitively expected, provided $J_2 = J_2' = J_R = 0$, a fully ferromagnetic order with $k_y = 0$ is stabilized if J_1 and J_1' are ferromagnetic and tend to infinity ($J_1, J_1' \to -\infty$). In contrast, a classical antiferromagnetic order with $k_y = 0.5$ is stabilized if these parameters are antiferromagnetic ($J_1, J_1' \to +\infty$) as presented in Fig. 3(a). The large green surfaces correspond to the $k_y = 0.25$ propagation vector, hence, to the up-up-down-down pattern typical of the block order. As expected, this peculiar ordering becomes the ground state as soon as J_1 and J_1' depart from each other. The symmetry with respect to the diagonal $J_1 = J_1'$ is due to the symmetric role of J_1 and J_1'. The block order is eventually obtained by taking into account J_2' and J_2, which couple the two legs of the ladder. The map presented in Fig. 3(b) shows the propagation vector along the ladder for a set of J_1' and J_1, which stabilizes the up-up-down-down sequence. The values used for J_1', J_1, and J_R are given in Table II. Interestingly, the block order remains stable provided that J_2' or J_2 is antiferromagnetic. This indeed contributes to the stabilization of identical up-up-down-down patterns in adjacent legs.
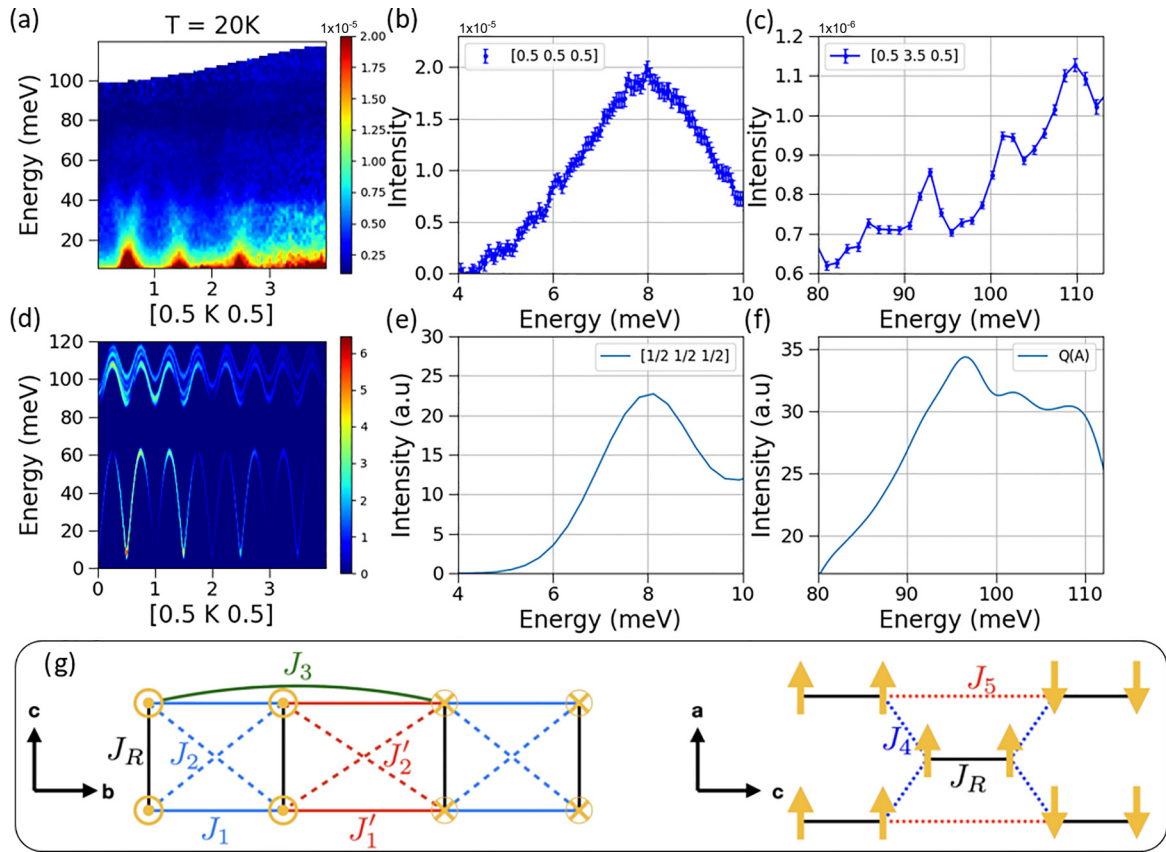
FIG. 2. (a) Color map showing the dispersion along (1/2, K, 1/2) at 20 K ($E_i = 125$ meV). Neutron intensity is on the logscale. (b) Experimental energy cut at $Q = (1/2, 1/2, 1/2)$ taken at 20 K ($E_i = 25$ meV). The elastic line was removed (see Ref. [11]). (c) Experimental energy cut at $Q = (1/2, 7/2, 1/2)$ taken at 20 K ($E_i = 125$ meV). The integration range in Qspace was adapted to improve visibility ($\Delta h = 0.5$, $\Delta k = 0.5$, and $\Delta l = 10$). (d) Simulated color map of $S_{SWT}(Q, \omega)$ along (1/2, K, 1/2). Intensity is on the logscale. (e) and (f) Simulation of the energy cut at $Q = (1/2, 1/2, 1/2)$. (g) Schematic sketch of the magnetic structure and the different exchange interactions used in the simulation. Left: Projection on the (b) and (c) plane. Right: Projection on the (a) and (c) plane. The crystallographic axis corresponds to the *Pnma* space-group setting.

Having reduced the possible range for relative exchange interaction strengths stabilizing the ground state, the spin dynamics was simulated using linear spin-wave theory [12]. Each coupling constant J_i was varied independently from the others within the appropriate region of the Monte Carlo phase diagram to disentangle their role in shaping the dispersion. First, J_1, J_R, and J_2 mainly affect the optical modes bandwidth
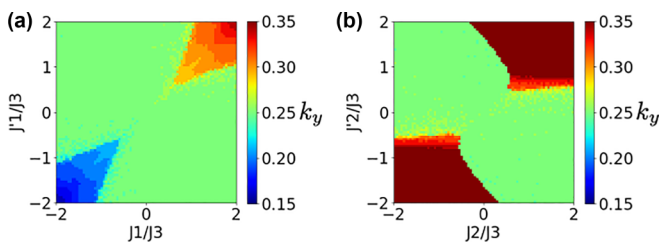

FIG. 3. Phase diagram obtained based on the propagation vector determined by Metropolis-Hasting simulations of a single ladder as a function of different couplings. The color scale indicates the value of k_y along the ladder. In (a), the calculations are performed for $J_2 = J_2' = J_R = 0$, whereas, in (b), J_1, J_1', and J_R values are given in Table II.

and energies. J_3, J_1', and J_2' affect both acoustic and optical modes. Finally, J_4, J_5, and the local anisotropy have an effect on the low-energy gap of the acoustic mode. The local anisotropy axis orientation $\mathbf{n}_i$ has been chosen to reproduce the umbrellalike magnetic ground state [4] with especially a nonzero component along both the b and the c directions. The exchange couplings that best fit the experiment are listed in Table II. The simulated dispersion is represented Fig. 2(d). As can be seen, the acoustic branches are well reproduced and the three optical modes are present. Using the same values, we simulated the energy cut at $Q = (1/2, 1/2, 1/2)$, displayed in Fig. 2(e), and showing a good agreement with the experimental cut displayed in Fig. 2(b). A powder average has been performed for the high-energy branches to compare with the large q integration of the experimental cut shown in Fig. 2(c).

TABLE II. Values of exchange interactions (in meV) determined using a purely antiferromagnetic effective Heisenberg model.

J_1	5.5	J_R	1.3	J_4	0.15
J_1'	19.2	J_2'	18.4	J_5	2.0
J_3	15.3	J_2	6.3	D	−3.9

As can be seen in Fig. 2(f), the three experimental modes are reproduced.

In the present model, the block order is stabilized by strong J_1', J_2', and J_3. The other couplings are weaker and frustrated. This is at variance with the model proposed in Ref. [7], which assumes the existence of alternating ferromagnetic and antiferromagnetic couplings along each leg of the ladder. Note that single-ion anisotropy is also relatively strong in our model. This is at the origin of the strong gap at the magnetic zone center $q = (1/2, 1/2, 1/2)$. Based on our previous analysis of the influence of each coupling, these behaviors lead us to believe that optical modes are related to intrablocks and frustrated couplings, whereas, the acoustic mode is associated with interblock couplings and strong anisotropy. It is interesting to note that the energy of this gap nearly coincides with the low-energy phonons observed in infrared spectroscopy around $60 \, \mathrm{cm}^{-1}$ [2]. This particular polar phonon mode seems to be affected by the magnetic ordering below T_N, suggesting a coupling with the magnetic excitations. Such coupling between phonon and magnon could indicate the presence of an electromagnon, the famous excitation bearing electroactive and magnetic characters [13,14].

III. DISCUSSION

The new set of exchange parameters determined in the present paper presents numerous advantages with respect to the previous proposed model [7]. First, all interactions being antiferromagnetic, the model is compatible with the Goodenough-Kanamori rule and the bonds angle listed in Table I. There is also no need to resort to ferromagnetic interaction, an artificial solution that remains rather difficult to justify physically. Second, the new set of parameters describes the three modes observed at high energy, and that were not resolved in the previous experiment performed on powder [7]. The strong amplitude of the nearest-neighbor coupling J_3 could be partially explained by the chemistry of the chalcogenide. Selenium orbitals are known to be particularly delocalized in space, likely responsible for this large second-neighbor interaction. In the same vein, sulfur orbitals are expected to be less delocalized, resulting in a weaker second-neighbor interaction in $BaFe_2S_3$. This explains why the nearest-neighbor frustrated coupling is lifted in this compound, leading to an antiferromagnetic stripelike order. Third, the magnetic transition observed under pressure in Ref. [5] finds a natural explanation in the present model. Indeed, as shown by Monte Carlo calculations, the magnetic propagation wave vector is quite sensitive to the J_1/J_3 ratio with the stripelike phase being found when J_3 decreases. The intuitive decrease in J_3 upon pressure is further supported by first-principles calculations performed on the parent compounds of $BaFe_2Se_3$, namely, FeSe and FeTe [15]. The authors claim that under pressure, the ground state of these systems transitions to an antiferromagnetic stripe order, as is the case for $BaFe_2Se_3$ at 4 GPa. However, detailed calculations of the exchange couplings would be helpful: Their evolution as a function of pressure is related to the structure in a nontrivial way. Fourth, the model detailed in this paper explains the stripe antiferromagnetic order observed in all other members of the series with similar structure [3,9,10]. Finally, the frustration inherent to this model provides a key ingredient to elucidate the magnetoelectric coupling in this system. Indeed, it has been shown that this compound is multiferroic [1,2,16] and exhibits a significant structural change across the Néel temperature with an increased deviation from the nonpolar average space group [1]. Although the magnetic structure chirality reported recently suggests that the inverse Dzyaloshinski-Moriya interaction could be a relevant ingredient at play [4], the presence of frustration suggests that an exchange-striction mechanism could also be at work. This reinforces the picture of a strong magnetoelastic coupling in these systems as suggested in Ref. [2].

IV. CONCLUSION

In conclusion, on the basis of single-crystal inelastic neutron-scattering experiments, is inferred an antiferromagnetic Heinsenberg model, providing a natural explanation for numerous properties observed in this quasiunidimensional iron-based multiferroic compound. This new model can be easily extended to other members of the family by tuning the parameters to describe the underlying magnetic orders. It would be interesting to revisit the already published spin dynamics data [17,18] in light of this new model and use it also for future studies of magnetic excitations. This result finally provides a new starting point to study the remarkable properties of these systems, among which multiferroicity and superconductivity.

[1] W. Zheng, V. Balédent, M. B. Lepetit, P. Retailleau, E. V. Elslande, C. R. Pasquier, P. Auban-Senzier, A. Forget, D. Colson, and P. Foury-Leylekian, Phys. Rev. B **101**, 020101(R) (2020).

[2] M. J. Weseloh, V. Balédent, W. Zheng, M. Verseils, P. Roy, J. B. Brubach, D. Colson, A. Forget, P. Foury-Leylekian, and M.-B. Lepetit, J. Phys.: Condens. Matter **34**, 255402 (2022).

[3] J. M. Caron, J. R. Neilson, D. C. Miller, K. Arpino, A. Llobet, and T. M. McQueen, Phys. Rev. B **85**, 180405(R) (2012).

[4] W. G. Zheng, V. Balédent, E. Ressouche, V. Petricek, D. Bounoua, P. Bourges, Y. Sidis, A. Forget, D. Colson, and P. Foury-Leylekian, Phys. Rev. B **106**, 134429 (2022).

[5] W.-G. Zheng, V. Balédent, C. V. Colin, F. Damay, J.-P. Rueff, A. Forget, D. Colson, and P. Foury-Leylekian, Commun. Phys. **5**, 183 (2022).

[6] J. Ying, H. Lei, C. Petrovic, Y. Xiao, and V. V. Struzhkin, Phys. Rev. B **95**, 241109(R) (2017).

[7] M. Mourigal, S. Wu, M. B. Stone, J. R. Neilson, J. M. Caron, T. M. McQueen, and C. L. Broholm, Phys. Rev. Lett. **115**, 047401 (2015).

[8] J. Herbrych, N. Kaushal, A. Nocera, G. Alvarez, A. Moreo, and E. Dagotto, Nat. Commun. **9**, 3736 (2018).

[9] T. Hawai, Y. Nambu, K. Ohgushi, F. Du, Y. Hirata, M. Avdeev, Y. Uwatoko, Y. Sekine, H. Fukazawa, J. Ma *et al.*, Phys. Rev. B **91**, 184416 (2015).

[10] H. Takahashi, A. Sugimoto, Y. Nambu, T. Yamauchi, Y. Hirata, T. Kawakami, M. Avdeev, K. Matsubayashi, F. Du, C. Kawashima, H. Soeda, S. Nakano, Y. Uwatoko, Y. Ueda, T. J. Sato, and K. Ohgushi, Nat. Mater. **14**, 1008 (2015).

[11] See Supplemental Material at http://link.aps.org/supplemental/10.1103/PhysRevB.108.014416 for sample characterization, data analysis and Monte Carlo calculation details.

[12] S. Petit, Collection SFN **12**, 105 (2011).

[13] S. Petit, V. Balédent, C. Doubrovsky, M. B. Lepetit, M. Greenblatt, B. Wanklyn, and P. Foury-Leylekian, Phys. Rev. B **87**, 140301(R) (2013).

[14] A. Vaunat, V. Balédent, S. Petit, P. Roy, J. B. Brubach, G. Giri, E. Rebolini, P. Steffens, S. Raymond, Q. Berrod, M. B. Lepetit, and P. Foury-Leylekian, Phys. Rev. B **103**, 174434 (2021).

[15] J. K. Glasbrenner, I. I. Mazin, H. O. Jeschke, P. J. Hirschfeld, R. M. Fernandes, and R. Valentí, Nat. Phys. **11**, 953 (2015).

[16] K. Du, L. Guo, J. Peng, X. Chen, Z.-N. Zhou, Y. Zhang, T. Zheng, Y.-P. Liang, J.-P. Lu, Z.-H. Ni, S.-S. Wang, G. Van Tendeloo, Z. Zhang, S. Dong, and H. Tian, npj Quantum Mater. **5**, 49 (2020).

[17] M. Wang, M. Yi, S. Jin, H. Jiang, Y. Song, H. Luo, A. D. Christianson, C. de la Cruz, E. Bourret-Courchesne, D.-X. Yao, D. H. Lee, and R. J. Birgeneau, Phys. Rev. B **94**, 041111(R) (2016).

[18] M. Wang, S. J. Jin, M. Yi, Y. Song, H. C. Jiang, W. L. Zhang, H. L. Sun, H. Q. Luo, A. D. Christianson, E. Bourret-Courchesne, D. H. Lee, D.-X. Yao, and R. J. Birgeneau, Phys. Rev. B **95**, 060502(R) (2017).